C. R. Physique 12 (2011) 141–150

Contents lists available at ScienceDirect

Comptes Rendus Physique

www.sciencedirect.com

Propagation and plasmas: new challenges, new applications

Ion acceleration in antiparallel collisionless magnetic reconnection: Kinetic and fluid aspects

Accélération des ions dans la reconnexion magnétique antiparallèle, aspects cinétiques et fluides

Nicolas Aunai *, Gérard Belmont, Roch Smets

Laboratoire de physique des plasmas, École polytechnique, route de Saclay 91128 Palaiseau cedex, France

ARTICLE INFO

Keywords:
Magnetic reconnection
Ion acceleration
Fluid and kinetic physics

Mots-clés :
Reconnexion magnétique
Accélération ionique
Physique fluide et cinétique

ABSTRACT

Using a two-dimensional hybrid simulation code, we study the ion acceleration in the vicinity of the ion decoupling region of collisionless magnetic reconnection. We investigate the fluid consequences of the observed kinetic phenomena and discuss to what extent it could be accounted for in fluid modeling. The initial setup is an antiparallel current sheet in a plasma with homogeneous density. We discuss the different forces acting on the ion bulk and show that the two dominant ones are the Hall electric force and the pressure force acting against each others. A dynamic equilibrium, which might also exist in fluid simulations, is here given by a kinetic effect. We therefore explain this pressure by an analysis of the ion distribution function and show that these are the result of an electrostatic bounce motion of the particles between the separatrices. This bounce motion is a characteristic of the ion decoupling region and therefore the resulting pattern of the pressure tensor may be considered as an additional observable feature of antiparallel reconnection in satellite data.

RÉSUMÉ

A l'aide d'un code de simulation hybride bi-dimensionnel, nous étudions la zone de découplage ionique créée lors de la reconnexion magnétique non collisionnelle. Nous examinons les conséquences fluides des phénomènes cinétiques observés et discutons dans quelle mesure ils peuvent être expliqués d'un point de vue fluide. La configuration initiale est une couche de courant antiparallèle dans un plasma de densité homogène. Nous discutons les différentes forces agissant sur le fluide ionique et montrons que les deux contributions dominantes sont la force électrique Hall et la force de pression agissant l'une contre l'autre. L'équilibre dynamique, qui peut également se trouver dans des simulations fluides, est ici engendré par un effet cinétique. Nous étudions donc cette force de pression par une analyse des fonctions de distribution et montrons que celles-ci résultent d'un mouvement de rebond électrostatique des ions sur les séparatrices. Ce mouvement de rebond est caractéristique de la zone de découplage ionique et le tenseur de pression

* Corresponding author.
E-mail addresses: nicolas.aunai@lpp.polytechnique.fr (N. Aunai), gerard.belmont@lpp.polytechnique.fr (G. Belmont), roch.smets@lpp.polytechnique.fr (R. Smets).

1631-0705/$ – see front matter
doi:10.1016/j.crhy.2010.11.004

des ions en résultant peut alors être considéré comme une nouvelle observable de la reconnexion magnétique non collisionnelle dans les données obtenues par satellite.

1. Introduction

Magnetic reconnection is a plasma process by which magnetic connectivity can be changed along the field line motion and magnetic energy transferred into bulk and thermal kinetic energy. It is thus of great importance in the dynamics of many astrophysical and laboratory systems such as the stellar/solar environments, planetary magnetospheres and Tokamak fusion devices. One of the key questions regarding magnetic reconnection concerns the rate at which the magnetic flux is being reconnected for a given system. Considering the assumption of steadiness, the Sweet–Parker scaling theory [1] predicts, in the resistive MHD framework, that the reconnection rate, evaluated by the out-of-plane electric field in 2D configurations, scales like $\eta^{1/2}$ where η is the collisional resistivity. In space plasmas, the resistivity is usually completly negligible and thus the Sweet–Parker reconnection rate is throttled at unrealistic values. In collisionless systems, the successive decoupling of the ions and the electrons from the magnetic field creates a completly different dynamics that has been observed to allow fast magnetic reconnection ([2] and references therein). While the ions decouple from the magnetic field at a scale comparable to the ion skin depth $\delta_i = c/\omega_{pi}$, the electrons are still magnetized and keep drifting toward the X point. Eventually, they decouple from the magnetic field and are accelerated by the reconnection electric field at much smaller scales. This electron acceleration and re-coupling give rise to strong currents which turn on the Hall term in the induction equation and drag the newly reconnected field lines in the out-of-plane direction and eject it downstream in a way comparable to the whistler wave dynamics [2–4]. This property makes the reconnection rate roughly independent of the electron to ion mass ratio, i.e. of the electron decoupling mechanism [2]. The direct observational consequence of this process is the quadrupolar out-of-plane magnetic field created around the X point, and a strong bipolar Hall electric field mapping the separatrices close to the X point. In this region, the ions are not tied to the field lines, they can thus move through the wide bottleneck opened by the Hall effect. It is thus the bulk ion motion and its coupling to the Hall fields that controls the reconnection rate. For antiparallel reconnection, it is generally found that the ions accelerate up to a fraction of the upstream Alfvén speed within $\sim 10\delta_i$ no matter how large the system is [5,6]. This bulk acceleration is thought to be given by the Hall electric force. However some discrepancies exist between Hall MHD and kinetic models [5,7]. Kinetic features have also found to be ubiquitous in the ion decoupling region [8–12]. Understanding the ion physics in the vicinity of the decoupling region thus appears to be important, and in particular, it seems necessary to discuss the relationship between kinetic processes and the resulting bulk acceleration.

Ignoring the two-fluid effects, test particle simulations [13,14] and analytical studies [15] have made several predictions concerning the ion particle dynamics in a magnetic reconnection topology. These studies lead to the conclusion that Speiser-like trajectories [15] are the mechanism by which ions gain kinetic energy. In this mechanism, incoming ions are decoupled from the magnetic field because their Larmor radius is larger than the field line curvature radius. While decoupled, they describe a meandering motion because of the field reversal, accelerate along the reconnection electric field and in the mean time, turn away in the downstream direction because of the Lorentz force given by the normal magnetic field. Features in distribution functions observed in self-consistent kinetic numerical simulations downstream of the X line [12,11,10], as well as the evolution of the energy of accelerated ions [16], have been interpreted as the evidences of the Speiser mechanism predicted earlier.

However, when it comes to understand the ion dynamics in the decoupling region (i.e. close to the X point), things are likely to be different. The Hall electric field resulting from the electronic motion of the field lines close to the X point is much larger than the reconnection electric field, and thus cannot be neglected. It has been said to be responsible for the bulk acceleration and particle acceleration [8]. However, these two points of view are a priori not equivalent, and if they are often discussed, they are rarely confronted against each other. It is not clear to what extent kinetic features are related to bulk motion.

In the Earth magnetosphere, satellite data have been several times interpreted in terms of collisionless magnetic reconnection. In particular, magnetic field consistent with the Hall quadrupole and also strong bipolar electric field have been observed consistently [17,21,18–20]. Wygant [20] have presented a detailed analysis of satellite data interpreted as a magnetic reconnection event, and in particular discussed the ion acceleration in the decoupling region from both particle and fluid points of view. In this event, cold ionospheric ions are accelerated by the normal Hall electric field and describe an electrostatic bounce motion which produces two counterstreaming beams in the normal direction. While they did not exclude that the physics may differ from one plasma regime to another, Wygant [20] explained that the Hall electric field is the primary cause for the decoupling and acceleration of ions in the event they have studied. From the fluid point of view, the counterstreaming beams mainly create a pressure force opposed to the normal Hall electric force. Wygant [20] also discussed how the particles can transfer the velocity gained from the Hall field in the downstream direction to create the fluid jet.

Counterstreaming beams have already been noticed in kinetic simulations of magnetic reconnection [8,10,22,11,23] as well as magnetotail reconnection events [20] or even solar wind reconnection events [24], but the physical phenomenon

behind this feature may differ from one case to the other and is not necessarily related to the ion decoupling region physics. For example, Gosling et al. [24] reported an observation of solar wind reconnection. They have identified cold counterstreaming beams which were interpreted as interpenetrating populations entering the exhaust from opposite upstream regions. The exhaust region they have studied had an estimated width that far exceeds the upstream ion inertial length or Larmor radius and is thus located at a great distance from what is usually called the ion decoupling region. Drake et al. [25] studied the ion heating downstream of the X line as a consequence of Speiser-like trajectories of lobe ions entering the exhaust. Their study focused on processes far in the downstream region where the electric field is the MHD convection field. They observed counterstreaming beams and discussed them in term of Speiser-like trajectories. In the decoupling region, counterstreaming beams have been reported by several authors (e.g. [10,22,26,8]) and often linked to the presence of the Hall electric field. Hoshino et al. [10] and Shay et al. [8] explained how ions accelerated in the decoupling region mix with other populations downstream and create non-Maxwellian beam features.

In this article, we present a 2D hybrid simulation investigating ion acceleration in collisionless antiparallel magnetic reconnection in the vicinity of the ion decoupling region. Other effects may appear outside of this region, and are not the topic of this paper. The simulation results illustrate the observation made by Wygant [20] and focus on the relation between particle acceleration and fluid acceleration/heating related to the presence of the Hall fields. The first section of this article is devoted to the description of the simulation model and initial conditions. In the second section, we calculate the different terms contributing to the ion momentum equation and show the importance of the ion pressure force. We show that this ion pressure force is given in our simulation by a temperature tensor effect rather than a density compression. In particular, we show that the off-diagonal part of the pressure tensor exhibits a quadrupolar structure around the X point, so that the associated force almost balances the x component of the electric field, not observed by Wygant [20]. In the dynamics of collisionless plasmas, the concept of temperature tensor is highly related to the shape of the distribution function and thus to microphysics. We therefore explain these pressure forces in section three by an analysis of the ion distributions in the decoupling region. We show by a detailed analysis of ion trajectories that the distributions and so the pressure force indeed comes from a bounce motion of the ions in the electrostatic potential well resulting from the Hall effect. As one moves further from the X point, where the bounce motion does not exist anymore, off-diagonal terms of the pressure tensor also exist but are related to the mixing of the local frozen-in population with a fast population accelerated in the decoupling region [10,8]. For steady reconnection, the pressure tensor, is therefore highly related to the ion dynamical regime and this property can be considered as an additional observable proxy of the decoupling region. Our findings about the ion dynamics in the decoupling region is directly comparable to what really happens in symmetric collisionless reconnection events [20]. Section four summarizes our results and discusses future work.

2. Simulation model and initial setup

Considering the ion acceleration, we use the hybrid formalism, in which only ions are treated as particles. The numerical scheme is close to those described in [27,28]. The ion motion is calculated with Eq. (1), where $\mathbf{v}_{pi}$ is the particle velocity. This equation is solved using the Boris algorithm with a standard leapfrog scheme. Electrons are considered as a fluid with inertia, and their momentum equation (2) is providing the electric field. The electron inertia is added using the standard method of the pseudo fields [29,30] and the resulting elliptic equation is solved with an iterative method using the parallel PETSc library.[1] In Eq. (2), the total current is given by Ampere's law (4) where we have neglected the displacement current. The magnetic field is updated via Faraday's equation (3). The electron fluid is supposed to be isothermal and isotropic. The electromagnetic fields are solved on two uniform cartesian staggered grids. The equations are discretized with a second order finite differences method and updated with the predictor-corrector scheme.

$$m_i \frac{\mathrm{d}\mathbf{v}_{pi}}{\mathrm{d}t} = e(\mathbf{v}_{pi} \times \mathbf{B} + \mathbf{E}) \tag{1}$$

$$\mathbf{E} = -\mathbf{v}_i \times \mathbf{B} + \frac{1}{ne}(\mathbf{j} \times \mathbf{B} - \nabla P_e) - \frac{m_e}{e}\frac{\mathrm{d}\mathbf{v_e}}{\mathrm{d}t} \tag{2}$$

$$\frac{\partial \mathbf{B}}{\partial t} = -\nabla \times \mathbf{E} \tag{3}$$

$$\nabla \times \mathbf{B} = \mu_0(\mathbf{v}_i - \mathbf{v}_e) \tag{4}$$

Distances are normalized to the ion inertial length $\delta_i = c/\omega_{pi} = V_A/\Omega_{ci}$ and time to the inverse of the ion cyclotron frequency Ω_{ci}^{-1}. The magnetic field and density are normalized to arbitrary values $\mathbf{B}_0$ and n_0 which in this paper are the asymptotic values. In these units, the simulation domain is a rectangle $(x_m, y_m) = (280, 40)$ with $n_x = 1024$ and $n_y = 512$ cells in x and y directions. We set about 100 particles per cell initially, that is about 4000 particles per δ_i^2. The ion to electron mass ratio is set to $m_i/m_e = 50$, so that the electron inertial length is $\delta_e = 0.14\delta_i$. Perfect conducting boundary conditions are used at y borders and periodic in the x direction. It is well known that periodic boundary conditions can limit the time during which the simulation is valid. For that reason we pay attention to the fact that the box is long enough

[1] http://www.mcs.anl.gov/petsc.

in the downstream direction (x) and wide enough in the upstream direction (y), so that neither recirculation effect or depletion of inflowing magnetic flux changes the reconnection process.

The initial magnetic field profile is antiparallel (with no guide field) and $\mathbf{B} = B_0 \tanh((y - 0.5y_m)/\lambda)\mathbf{e}_x$ with the half-width $\lambda = 1$ and $B_0 = 1$. The density is uniform with $n_0 = 1$. The total β of the plasma is set to 0.1 and the electron temperature is uniform and set to $T_e = 0.005$. Ions are loaded in a local Maxwellian distribution function, their temperature is chosen to balance the total pressure. The asymptotic ion temperature is thus $T_i = 0.045$ and the sheet temperature is $T_i = 0.545$. For the sake of observational comparison, let's note that if one takes $B_0 = 15nT$, $n_0 = 0.25$ cm^{-3}, the ion temperature is 250 eV and 2.4 keV in the asymptotic region and sheet, respectively. This initial condition is not a Vlasov–Maxwell equilibrium and small waves are emitted from the current sheet at the very beginning of the simulation ($\Omega_{ci} < 1$). These wave are the consequence of the kinetic relaxation of the current sheet, propagate in the y direction and are eventually reflected back to the sheet from the conducting walls at a time long compared to the X point dynamics ($\Delta t \Omega_{ci} \approx 50$). Finally, in order to have one major X point in the simulation box, we impose a magnetic perturbation localized at the center of the domain. Let us note that some comparable wave activity has been reported before (e.g. [31]), although the authors have initialized their simulation with the Harris equilibrium [32]. This is likely to be due to the initial magnetic perturbation inevitably, leading to wave emission as long as one does not know how to create one proper eigenmode of the current sheet.

3. Fluid acceleration

It is generally accepted that the ion outflow velocity scales like the Alfvén speed based on the upstream plasma parameters. In the collisionless antiparallel case, a comparable speed is found to be reached within a microscopic distance which might not depend on the system size [9]. This strong bulk acceleration is generally said to result from the interaction with the Hall electric field that develops on the separatrices [8,5]. However, when the simulation domain is large enough so that neither artificial pile-up nor recirculation effect changes the outflow velocity, it has been noticed in kinetic simulations that the outflow velocity is significantly below the upstream Alfvén speed [33,5]. Moreover, Shay et al. [5] compared Hall MHD and hybrid results and showed that, for the same reconnection rate, the hybrid outflow channel is twice as wide as the MHD one, and the outflow speed is half that of the MHD case. The key point for proton dynamics is to understand the physics involved in the transfer of electromagnetic energy into bulk and thermal energy. The goal of this section is to investigate the coupling of the Hall electric field to the ions and the resulting bulk acceleration. The ion acceleration is given by the ion momentum equation (5), where $\mathbf{v}_i$ is the ion fluid velocity, n is the density, m_i the ion mass, $\mathbf{E}$ and $\mathbf{B}$ the electric and magnetic field, and $\mathbf{P_i}$ is the full ion pressure tensor.

$$m_i n \frac{\partial \mathbf{v}_i}{\partial t} + m_i n \mathbf{v}_i \cdot \nabla \mathbf{v}_i = -\nabla \cdot \mathbf{P}_i + ne\mathbf{E} + ne\,\mathbf{v}_i \times \mathbf{B} \tag{5}$$

The Hall electric field $-\mathbf{v}_e \times \mathbf{B}$ is dominantly directed toward the center of the current sheet, but has a small component pointing in the downstream region. This small E_x component is color coded in Fig. 1.a whereas E_y is shown in Fig. 1.b. E_x is located around the X point, with a magnitude about $0.1V_AB_0$. E_y is stronger around the X point ($\sim 0.7V_AB_0$) and still exists further away with a weaker amplitude. Close to the X point, the electric field is mostly associated to the motion of the magnetic field lines frozen in the electron fluid while further away it is related to the field line motion frozen in the whole plasma [11,25]. Fig. 2.a is a slice of the different terms of Eq. (5) in the x direction at $t = 100$ and $x = 148.5$. The choice of the location $x = 148.5$ has been motivated by the fact that the Hall electric field still exists, and the contribution of each separatrix can there be distinguished properly thanks to their separation. However, the behavior of the fluid is found to be the same (not shown) down to the X point. The time $t = 100$ is chosen because the unsteady region associated to the leading piled-up reconnected field line is far enough so that it is believed not to perturbate the physics in the decoupling region. At this time however, a large amount of magnetic flux has already been reconnected so that the upstream density and magnetic flux are significantly below the initial values. The consequence is that the raw reconnection rate is smaller than at the beginning of the simulation. This does however not change the present qualitative discussion nor the ratios between the different terms in the ion momentum equation. In addition, one has to notice that small magnetic islands (of size $\sim 3\delta_i$) are regularly ejected from the reconnection region (not shown) and change locally the force balance. We will not discuss this effect any further since we are, in this paper, only interested about quasi-steady features (compared to the simulation duration). In satellite data, depending on their production rate, these islands might complicate the observation of the steady structure we are discussing about.

Back in Fig. 2.a, we observe as expected a strong and positive electric force neE_x located on the separatrices (green curve). The magnetic force $en(v_{iy}Bz - v_{iz}By)$ is also strong at this location making the fluid turn around the magnetic field. This does not provide kinetic energy but nevertheless transfers the acquired velocity between different directions. One can note that there is a significant pressure force also located on the separatrices but with negative values (solid blue line). If we write the pressure tensor $\mathbf{P}_i$ in the form $\mathbf{P}_i \equiv n\mathbf{T}_i$, we can separate the role of the density of particles n from the role of the shape of the distribution function related to the microphysics/particle dynamics, the latter being described by the macroscopic tensor $\mathbf{T}_i$. The surprise here is that this pressure force does not correspond to a density gradient located on the separatrices, but is rather a kinetic effect since it is dominantly given by the off-diagonal part of the ion pressure tensor. This can be observed by comparing the dashed blue curve ($-\partial_y P_{ixy}$) to the solid one ($-\nabla_x \cdot P_i$). Fig. 2.b is a slice of

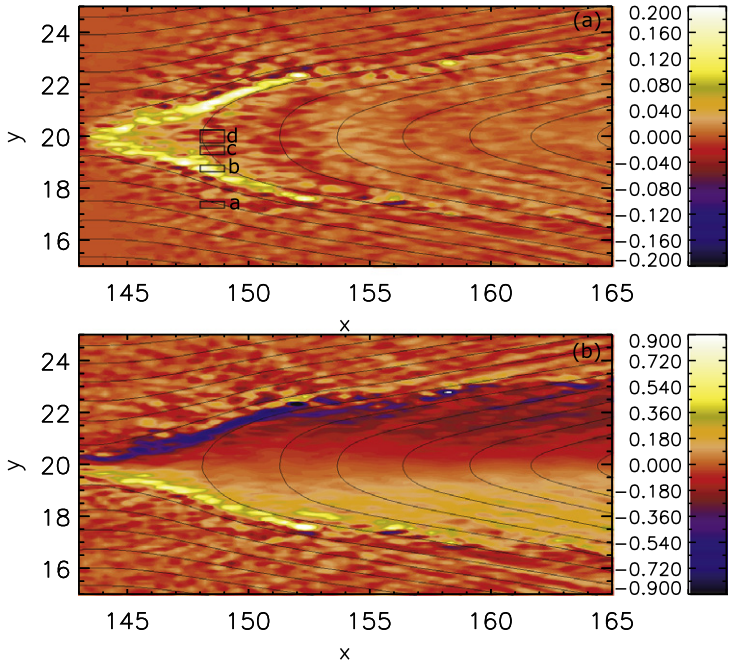

Fig. 1. a (top): y component of the electric field, **b** (bottom): x component of the electric field. In both panels the black lines represents the in-plane magnetic field lines. The boxes are the locations where the ion distribution functions shown in Fig. 4 are evaluated. Both figures are made at $t\Omega_{ci} = 100$.

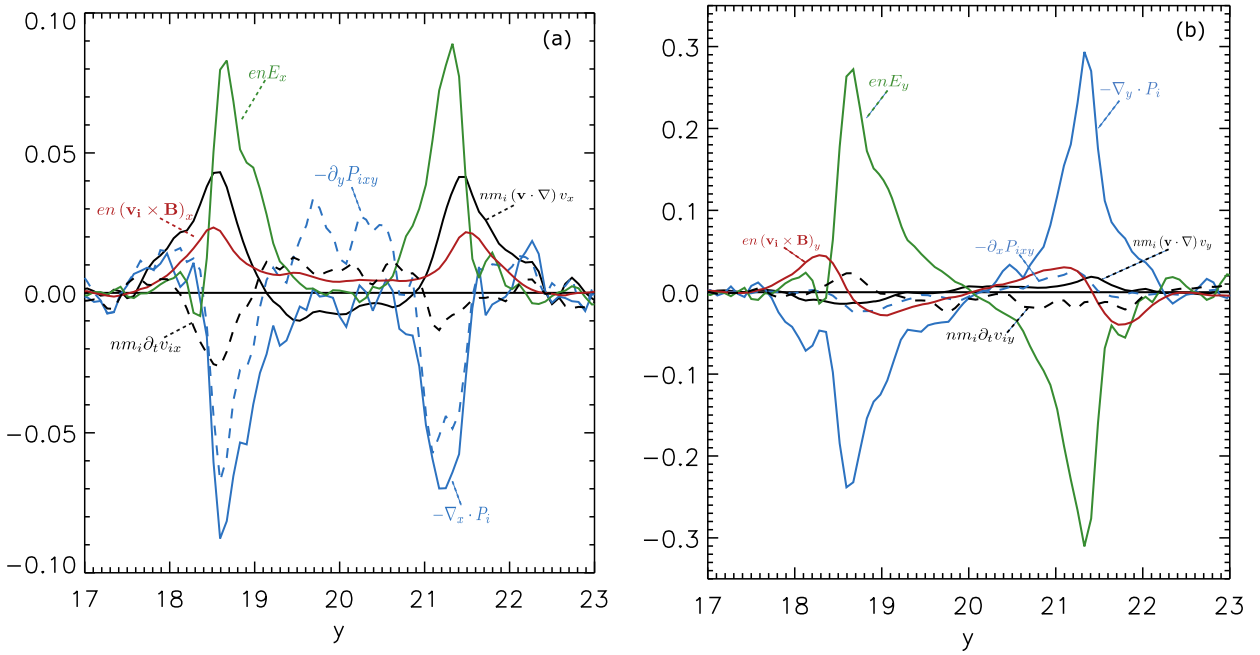

Fig. 2. Slice of the different terms in the ion momentum equation (5): **a**, in the x direction (left) and **b**, y direction (right). The green curve is the electric force $en\mathbf{E}$, the red curve is the Lorentz force $en\mathbf{v}_i \times \mathbf{B}$, and the solid blue curve is the total pressure force $-\nabla P_i$. The off diagonal contribution $-\partial_y P_{ixy}$ (right: $-\partial_x P_{ixy}$) to this pressure force is represented by the dashed blue line. The solid black line represents the steady acceleration $m_i n\mathbf{v}_i \cdot \nabla\mathbf{v}_i$ while the local acceleration $m_i n\partial_t \mathbf{v}_i$ is the dashed black curve.

the different terms of Eq. (5) in the y direction at the same location. The large inward electric force clearly appears to be balanced by the diagonal term of the pressure tensor $-\partial_y P_{iyy}$. It appears in both Figs. 2.a and 2.b that the acceleration is approximatly steady ($\partial_t \mathbf{v} \approx 0$) and that the electric force is almost entirely balanced by the pressure force for both in-plane components. Our simulation allows to explain the form of the pressure tensor, but the same pressure force is necessary whatever the fluid modeling. When a field line arrives on the separatrix, it is dragged at a great velocity by a fast steady

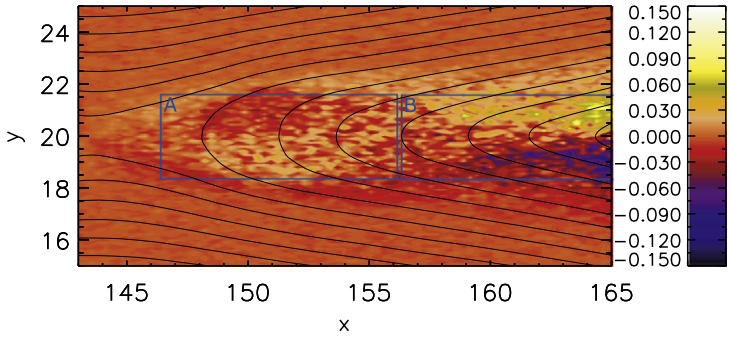

Fig. 3. Color coded P_{ixy} at $t = 100$. Black lines represent in-plane magnetic field lines. See text for details about region A and B.

frozen-in electron flow, leading to a strong electric field. On the ion fluid point of view, the frozen-in motion stops at the separatrix. Too heavy to follow the sudden motion of the field line, it however feels the resulting electric field. This electric field, pointing dominantly toward the center of the current sheet from the two opposite separatrices, compresses the fluid in the exhaust and increases the gas pressure rather than accelerates it. The observed pressure force is thus completly consistent with the symmetric geometry of the Hall electric field. However, the process supporting this pressure in a fluid modeling depends on the closure equation, and the resulting size of the steady structure is also dependant of this closure. In the hybrid formalism, the ions are treated as particles so that no closure hypothesis is done. In this context, it turns out that particle dynamics is the most important effect for the settlement of the dynamic quasi-equilibrium. This result differs from what could be obtained in a fluid simulation where the fluid closure would force the dynamic equilibrium to be preferentially given by a density gradient, and thus might change the width of the outflow channel, as observed by Shay et al. [5]. On the energy point of view, one can state that a large amount of electric energy is transfered to thermal energy via $-(\nabla \cdot \mathbf{P}_i) \cdot \mathbf{v}_i$.

Fig. 3 represents in color code the component P_{ixy} of the ion pressure tensor on the right side of the X point at $t = 100$. One can see in region **A** a bipolar signature consistent with the observed $-\partial_y P_{ixy}$. However this structure does not extent all along the downstream region. The sign of this component of the pressure tensor even changes further away (region **B**). This observation is made at $t = 100$ but is found at all times as long as the unsteady region created by the collision of the jet with the ambient sheet plasma has moved away and leaves a quasi-steady-sheet behind. By symmetry around the X point, the P_{ixy} component of the pressure tensor therefore has a quadrupolar structure in the vicinity of the ion decoupling region. The reason why its sign changes outside this region will become clear in Section 4. It is worth noting anyway that the quadrupolar structure of P_{ixy} can be considered as a characteristic feature of the ion decoupling region in collisionless antiparallel magnetic reconnection.

4. Particle dynamics and pressure tensor

In order to understand the structure of the pressure force represented in Fig. 2, it is helpful examining the distribution function of ions at different y locations for $x = 148.5$. Fig. 4 represents a projection of the ion distribution function in the $v_x - v_y$ plane located at each of the small white boxes seen in Fig. 1.a, from bottom to top. Distribution **a** is evaluated in the inflow region and is a cold $\mathbf{E} \times \mathbf{B}$ drifting Maxwellian. The in-plane fluid velocity is roughly perpendicular to the local magnetic field and directed toward the current sheet. Distribution **b** is located on the separatrix and is not Maxwellian anymore. The distribution consists there of two distinct populations: a small population with $v_y < 0$ and a large one with $v_y > 0$. A little bit further in the exhaust (distribution **c**) the two populations are even more separated and form two cold counterstreaming beams. At the center of the jet, the two beams are found to be equal and symmetric with respect to the $v_y = 0$ axis. Because of symmetry, on the other side of the $B_x = 0$ line, the situation is obviously found to be reversed (not shown). At each location, the magnetic field and the velocity have turned a bit more toward the normal and the outflow direction respectively. It is obvious from these figures that as one goes from upstream to the exhaust region, the appearance of counterstreaming beams effectively increases the temperature component T_{iyy}, thus creating the strong pressure gradient we observe in Fig. 2.b. This sudden increase of the temperature cannot be compared to a thermodynamical compression as in usual gases since no statistical equilibrium is reached in the exhaust. Nevertheless it still participates to the momentum balance in the same qualitative way than in a collisional plasma. At this point, the simulation results are comforting the Wygant [20] fluid interpretation of approximate pressure balance in the y direction. In distributions **b** and **c**, the larger v_x more particles are found at larger v_y, thus making a small but finite positive correlation between v_x and v_y, which is exactly what P_{ixy} is about. Of course P_{ixy} is zero for distribution **a** because it is isotropic. Therefore, from position **a** to position **b**, there is a positive derivative $\partial_y P_{ixy}$ explaining the negative contribution to the x pressure force. As noticed before, the distribution at the center of the exhaust is symmetric with respect to the $v_y = 0$ axis so $P_{ixy} = 0$ there. From position **c** to position **d**, there is therefore a negative derivative $\partial_y P_{ixy}$ so the contribution to the x component of the force is positive.

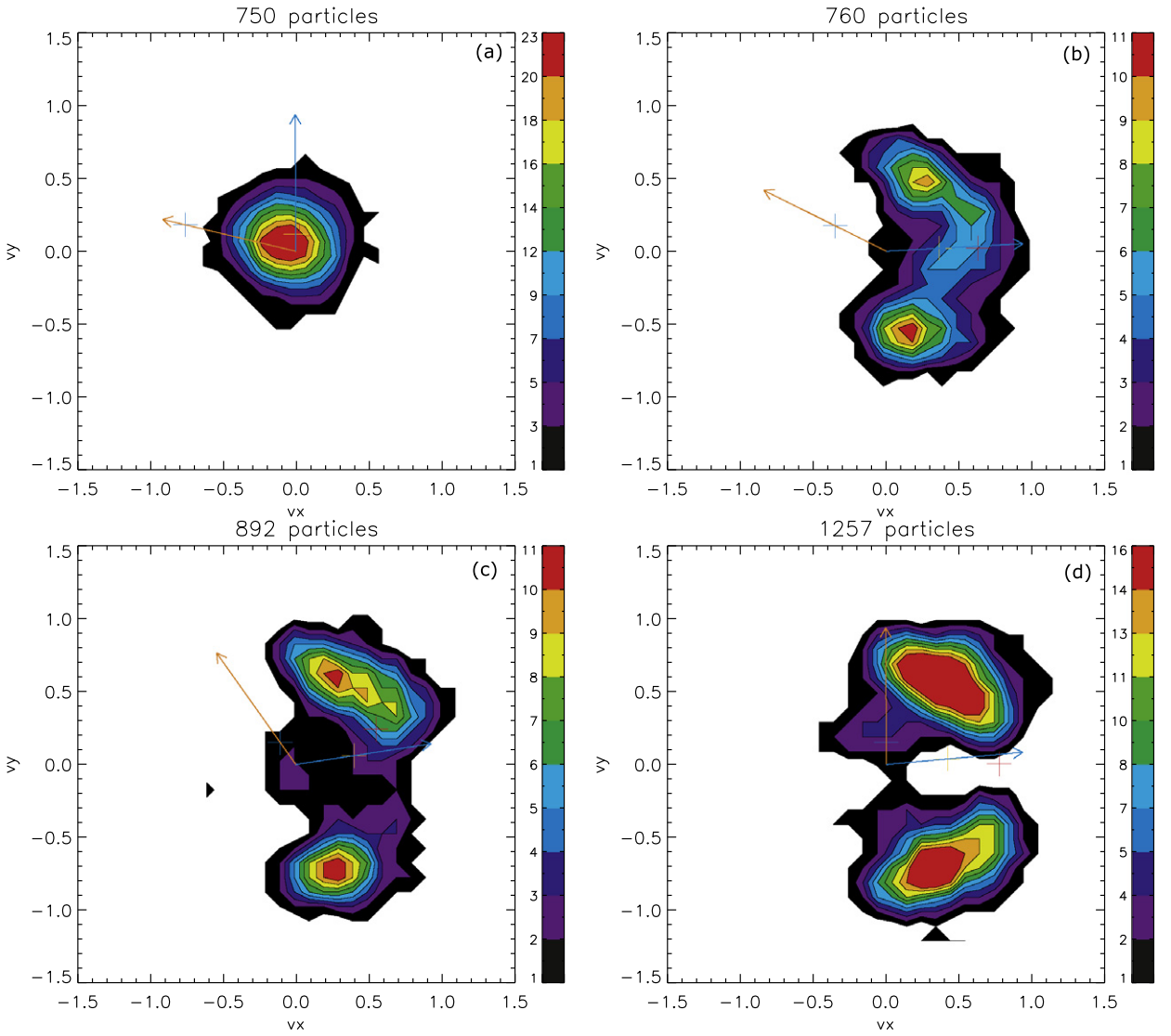

Fig. 4. Ion distribution functions evaluated in the little boxes seen in Fig. 1. Brown and blue arrows give the direction of the in-plane magnetic field and in-plane fluid velocity, respectively. The blue cross is the value of the in-plane Alfvén speed, the brown one represents the value of the in-plane fluid velocity, and the red one is the local in-plane $\mathbf{E} \times \mathbf{B}$ drift velocity.

To elucidate the mechanism behind the observed beams, let us look at the trajectory of particles contributing to these distributions, obtained self-consistently from the hybrid calculation. Fig. 5 represents the typical trajectory of a particle picked in the distribution **b**, superposed to the color coded x component of the electric field, at time $t = 100$. One clearly sees three phases in this trajectory. The first one consists of a magnetized drift motion. The second one begins when the particle reaches the top right separatrix and appears to describe a bounce motion within the exhaust region. Eventually on a third phase, the particle gets magnetized again, drifts with the reconnected field line and no longer bounce on both separatrices. A comparable trajectory is found for all particles picked in this distribution, which explains its beam structure. The bounce motion of the particle is further analysed in Fig. 6 where it is represented in different planes. In this figure, one clearly sees that the bounce motion is strongly related to the electric force and not to the magnetic force. This illustrates the Wygant [20] interpretation. Ions are greatly accelerated within the Hall potential well and describe an electrostatic bounce motion and not a magnetic meandering motion. In distributions **b** and **c**, the large $v_y > 0$ population consists of a mixing of particles that have interacted with the potential walls a different number of times: because of the divergence of the potential well, each reflection irreversibly transfer the velocity acquired from the potential from the y direction to the x one. The more reflections the particle has made, the larger its v_x component is and the smaller its v_y component is. This effect appears as a "dispersion" in velocity space in the $v_y > 0$ population and is well seen on distribution **b**, **c**, **d** for $v_y > 0$ populations. The small population in distribution **b** is in a ballistic motion previously accelerated by the opposite separatrix and not yet reflected. There is thus no dispersion for this population, i.e. it more or less conserves its original circular shape

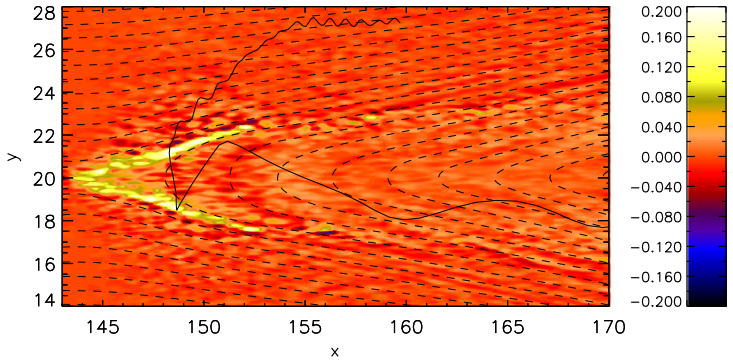

Fig. 5. Trajectory of a typical particle picked in distribution **b** represented as a solid black line superposed on the color coded E_x electric component at time $t = 100$. The dashed black lines represent the in-plane magnetic field lines.

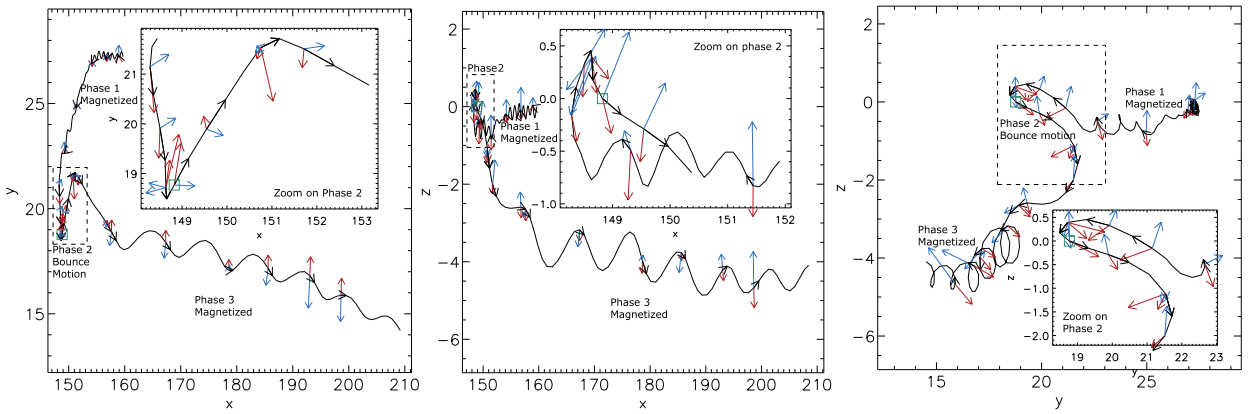

Fig. 6. Trajectory of the particle seen in Fig. 5 in the x–y plane (left), x–z plane (center) and y–z plane (right). In each panel the in-plane electric force and magnetic force are represented by red and blue arrows, respectively. The blue square is the location of the particle at the selection time.

in velocity space. In distribution **d**, which is in the middle of the sheet, the dispersion effect can be seen on both beams. This kinetic dispersion explains both the general in-plane correlation of the distribution function and the shape of each beam. Moreover it clarifies the kinetic origin of the off-diagonal component of the pressure force.

As said in Section 3, and shown in Fig. 3, the structure of the pressure component P_{ixy} changes as one moves away from the ion decoupling region. This can be easily understood. In Fig. 5, one can see that the accelerated particle gets magnetized again and stays on the same side of the $B_x = 0$ line. This particle, and all the similar particles, will eventually mix with particles coming from outside the current sheet and frozen-in the downstream reconnected field line. This mixing, also reported by Hoshino et al. [10] and Shay et al. [8], will result in a distribution that will exhibit a slow Maxwellian population with a fast population shifted in the parallel direction. Depending on the side of the $B_x = 0$ line, and thus on the direction of the magnetic field, it will appear in the ion pressure tensor with a non-zero bipolar P_{ixy} as observed in Fig. 3. In other words, this part of the pressure tensor in the downstream region can be seen as a consequence of the kinetic acceleration in the decoupling region. This effect is likely to become negligible far from the X point, when the particles accelerated in the decoupling region have been spread in phase space so that their contribution becomes insignificant compared to the particles of more local origin. In these remote regions, the exhaust boundary can be assumed to be more "MHD", i.e. the differences between distribution functions just upstream and just downstream of the discontinuity become mainly determined by local acceleration. It is likely to be the case in solar wind reconnection observations [24] where the exhaust is crossed very far away from the X line. However, such large distances cannot be properly observed with periodic simulation domains such as ours or the one presented by Drake et al. [25]. With these domain sizes, the downstream region is an intermediate one, where non-local acceleration and mixing effects both participate to the kinetic temperature, followed by a field piled-up region artificially created by the periodic boundaries.

5. Summary and discussion

In this paper, we have studied the ion interaction with the Hall electric field in the vicinity of the ion decoupling region in the antiparallel case of collisionless magnetic reconnection and discussed the relation between kinetic physics and fluid

interpretation. Our work shows to what extent the presence of non-Maxwellian signatures can be compatible with a fluid modeling:

- **The pressure force:** Our study reveals the important role played by the pressure force in the ion momentum equation. Indeed, the pressure force was found to balance a great part of the Hall electric force. The increase of the pressure within the exhaust is a consequence of the symmetric strong inward electric force that compresses the gas rather than accelerate it efficiently toward the exit. The Hybrid formalism does not impose a closure hypothesis for the ions, and the process supporting the pressure increase is found to be dominantly a kinetic one.
- **Counterstreaming beams:** As in previous papers, counterstreaming ion beams are found in this region. We have shown how these kinetic structures are related to the bulk acceleration by explaining how their shape is making the observed pressure force.
- **Particle dynamics:** We have detailed the particle dynamics behind these beams and find that the ions describe an electric bounce motion within the exhaust. This motion can be explained by their interaction with the diverging Hall potential well. The divergence of the well transfers the acquired velocity from the y direction to the x one. The mixing of particles having interacted a different number of times with the potential creates an apparent dispersion in the velocity space which is observed in simulated distribution functions. This finding confirms that the kinetic features seen in the vicinity of the ion decoupling region are not related to a Speiser-like mechanism, but is rather strongly coupled to the presence of the Hall electric field.
- **Observations:** Finally, these results are in good agreement with the interpretation of satellite data suggested by Wygant [20]. The quadrupolar structure of P_{ixy} is a characteristic feature of the ion decoupling region and thus can be considered as a good observational proxy of this region in satellite data.

The generality of our results may, however, be limited by several facts which should be evaluated in future works:

- **Guide field effect:** We have not considered the effect of a possible guide field in the initial condition. With a guide field, the ions may still be magnetized in the exhaust and not bounce anymore. Even if not strong enough to magnetize the ions, a guide field can alter significantly the symmetry of the Hall electric field [34] and so change the bounce dynamics.
- **Symmetry:** As strongly dependant of the symmetric Hall field configuration, the effects explained in this paper are possibly different when reconnection occurs within an asymmetric configuration, like at the magnetopause or in some solar wind cases. In these cases, the Hall fields are no longer symmetric and the asymptotic populations present initial differences in temperature and density which complicates even more the kinetic structures.
- **Initial temperature:** In our initial condition, the asymptotic population is rather cold compared to the potential electric energy of the Hall well, so that every particle is well trapped within the well. A different kinetic behavior might appear as one increases the asymptotic temperature. The initially cold particles are expected to behave like the ones in our study, but the initially hot particles may have enough energy to overcome the potential barrier and behave differently, perhaps by oscillating in the reversal magnetic field as described in the Speiser mechanism.
- **Secondary islands:** Several magnetic islands are created and ejected from the system as the reconnection proceeds. This unsteady behavior changes locally the force balance and depending on the production rate can make the observation of the background steady behavior quite difficult, or even make its interest questionable.

References

[1] E.N. Parker, Journal of Geophysical Research 62 (1957) 509.
[2] J. Birn, et al., Geospace Environmental Modeling (GEM) magnetic reconnection challenge, Journal of Geophysical Research 106 (2001) 3715–3720.
[3] M.E. Mandt, R.E. Denton, J.F. Drake, Transition to whistler mediated magnetic reconnection, Geophysical Research Letters 21 (1994) 73–76.
[4] J.F. Drake, M.A. Shay, M. Swisdak, The Hall fields and fast magnetic reconnection, Physics of Plasmas 15 (2008) 042306.
[5] M.A. Shay, et al., Alfvénic collisionless magnetic reconnection and the Hall term, Journal of Geophysical Research 106 (2001) 3759–3772.
[6] M.A. Shay, et al., The scaling of embedded collisionless reconnection, Physics of Plasmas 11 (2004) 2199–2213.
[7] L. Yin, D. Winske, Plasma pressure tensor effects on reconnection: Hybrid and Hall-magnetohydrodynamics simulations, Physics of Plasmas 10 (2003) 1595–1604.
[8] M.A. Shay, et al., Structure of the dissipation region during collisionless magnetic reconnection, Journal of Geophysical Research 103 (1998) 9165–9176.
[9] M.A. Shay, et al., The collisionless magnetic reconnection for large systems, Geophysical Research Letters 26 (1999) 2163–2166.
[10] M. Hosino, et al., Ion dynamics in magnetic reconnection: comparison between numerical simulations and Geotail observations, Journal of Geophysical Research 103 (1998) 4509–4530.
[11] K. Arzner, M. Scholer, Kinetic structure of the post plasmoid plasma sheet during magnetotail reconnection, Journal of Geophysical Research 106 (2001) 3827–3844.
[12] R.-F. Lottermoser, M. Scholer, A.P. Matthews, Ion kinetic effects in magnetic reconnection: Hybrid simulations, Journal of Geophysical Research 102 (1998) 4547–4560.
[13] L.R. Lyons, T.W. Speiser, Evidence for current sheet acceleration in the geomagnetic tail, Journal of Geophysical Research 87 (1982) 2276–2286.
[14] R. Smets, D. Delcourt, D. Fontaine, Ion and electron distribution functions in the distant magnetotail: Modeling of Geotail observations, Journal of Geophysical Research 103 (1998) 20407–20417.
[15] T.W. Speiser, Particle trajectories in model current sheets 1. Analytical solutions, Journal of Geophysical Research 70 (1965) 4219–4226.
[16] M.M. Kuznetsova, M. Hesse, D. Winske, Ion dynamics in a hybrid simulation of magnetotail reconnection, Journal of Geophysical Research 101 (1996) 27351–27374.

[17] T. Nagai, Geotail observations of the Hall current system: Evidence of magnetic reconnection in the magnetotail, Journal of Geophysical Research 106 (2001) 25929–25950.
[18] F.S. Mozer, S.D. Bale, T.D. Phan, Evidence of diffusion regions at a subsolar magnetopause crossing, Physical Review Letters 89 (2002).
[19] A. Vaivads, et al., Structure of the magnetic reconnection diffusion region from four-spacecraft observations, Physical Review Letters 93 (2004).
[20] J.R. Wygant, Cluster observations of an intense normal component of the electric field at a thin reconnecting current sheet in the tail and its role in the shock-like acceleration of the ion fluid into the separatrix region, Journal of Geophysical Research 110 (2005) 9206.
[21] J.P. Eastwood, Multi-point observations of the Hall electromagnetic field and secondary island formation during magnetic reconnection, Journal of Geophysical Research 112 (2007).
[22] W. Pei, R. Horiuchi, T. Sato, Ion dynamics in steady collisionless driven reconnection, Physical Review Letters 87 (2001) 235003.
[23] T. Nagai, Counterstreaming ions as evidence of magnetic reconnection in the recovery phase of substorms at the kinetic level, Physics of Plasmas 9 (2002) 3705–3711.
[24] J.T. Gosling, et al., Direct evidence for magnetic reconnection in the solar wind near 1 AU, Journal of Geophysical Research 110 (2005) 1107.
[25] J.F. Drake, et al., Ion heating resulting from pickup in magnetic reconnection exhausts, Journal of Geophysical Research 114 (2009) 5111.
[26] N. Singh, et al., Features of electron current layers: Comparison between three-dimensional particle-in-cell simulations and Cluster observations, Journal of Geophysical Research 115 (2010) 4203.
[27] D.S. Harned, Quasineutral hybrid simulation of macroscopic plasma phenomena, Journal of Computational Physics 47 (1982) 452–462.
[28] R. Smets, et al., Diffusion at the Earth magnetopause: enhancement by Kelvin–Helmholtz instability, Annales Geophysicae 25 (2007) 271–282.
[29] A.S. Lipatov, The Hybrid Multiscale Simulation Technology, Springer, 2002.
[30] P.A. Cassak, Catastrophe model for the onset of fast magnetic reconnection, PhD Thesis.
[31] K. Fujimoto, R.D. Sydora, Whistler waves associated with magnetic reconnection, Geophysical Research Letters 35 (2008) 19112.
[32] E.G. Harris, Nuovo Cimento 23 (1962) 115.
[33] H. Karimabadi, Multiscale structure of the electron diffusion region, Geophysical Research Letters 34 (2007).
[34] J.P. Eastwood, et al., Asymmetry of the ion diffusion region hall electric and magnetic fields during guide field reconnection: Observations and comparison with simulations, Physical Review Letters 104 (2010).